Dynamics of supercooled liquids in the vicinity of soft and hard interfaces

Fang He, Li-Min Wang, and Ranko Richert
Department of Chemistry and Biochemistry, Arizona State University, Tempe, Arizona 85287-1604, USA
(Received 1 December 2004; published 25 April 2005)

Using solvation techniques we explore the dynamics of nanoconfined and interfacial supercooled liquids near their glass transition temperatures. Confinement is accomplished by the use of porous glasses with pore diameters between 4 and 7.5 nm, and by microemulsions with droplet sizes between 2.6 and 5 nm. Via the attachment of the probe molecules to the inner surface of porous glasses filled with 3-methylpentane, the interfacial layer is measured selectively for different surface curvatures and shows an increase of the relaxation time by more than three orders of magnitude over that of the bulk liquid. This frustration is most pronounced at the pore boundary and decreases gradually across the first few nanometers distance away from the interface. Nanoconfinement realized by glass-forming microemulsions with the confining material being more fluid than the intramicellar droplets reverse the situation from frustrated dynamics in hard confinement to accelerated relaxation behavior in the case of soft boundaries. Without changing the size of the geometrical restriction of propylene glycol, hard versus soft boundary conditions changes the glass transition shift ΔT_g from +6 K to −7 K. The findings can be rationalized on the basis of certain interfacial dynamics which differ from bulk behavior, with the penetration of this effect into the liquid being governed by the length scale of cooperativity. This picture explains both the more disperse relaxation times in confinement and the dependence of the average relaxation time on pore size.

DOI: 10.1103/PhysRevB.71.144205 PACS number(s): 64.70.Pf, 68.15.+e, 68.05.Gh, 77.22.Gm

I. INTRODUCTION

The current interest in the behavior of liquids in confined spaces and at interfaces originates from a variety of motivations. Liquids in these situations are responsible for the transport of water and oil in soils and rocks, they influence material transport in cells and near membranes, they lubricate surfaces, and they exhibit structures and dynamics which are not well understood to date.[1] The melting point depression is a classical example of finite size effects on the thermodynamics of a liquid,[2] but a number of other changes away from any phase transition have been observed. For instance, the dynamics of liquids is usually slower near a solid surface or in confined spaces compared with the bulk counterpart.[3] This is particularly true in the case of the atomically smooth interfaces of a surface force apparatus, where the effective viscosities increase dramatically when the confined liquid layer is being reduced to thicknesses of only few molecular diameters.[4,5] It has been questioned that solidification in this situation results from confinement only,[6] and changes in density and structure may play a significant role. Confinement to more irregular geometries like rocks, clays, or porous silica leads to less dramatic changes regarding dynamics or viscosities,[7] but these materials display greater variability regarding confinement effects and a diminished control regarding the surface properties.[8]

As a liquid is taken to lower temperatures, the intermolecular interactions and the viscosities increase. In the case of supercooled liquids, crystallization does not interfere and the viscosity and structural relaxation times can be increased gradually, until a kinetic transition into the glassy solid state at T_g is achieved.[9] In the very viscous regime just above this glass transition temperature T_g, the effects of confinement to length scales of several nanometers and the vicinity to interfaces are often much more pronounced than with more fluid systems.[10] Early work on glass-forming liquids focused on molecular materials confined to porous glasses with pore diameters of 2.5 to 7.5 nm. In such samples, Jackson and McKenna observed a confinement induced shift of the glass-transition temperature T_g,[11] commonly defined by a relaxation time of 100 s or by a viscosity reaching 10^{13} Poise. More recently, free standing polymer films as thin as ~10 nm have attracted attention, because T_g shifts as large as −70 K have been observed,[12,13] and because polymer films are required to perform in similar situations as photoresists in semiconductor manufacturing.[14]

Glass-forming liquids are characterized by nonexponential relaxation patterns with the average relaxation time varying with temperature in a super-Arrhenius fashion.[15] A number of models aimed at rationalizing the glass-transition phenomenology involve length scales of cooperativity[16] or heterogeneity,[17–19] both claimed to be of order 3 ± 2 nm. Therefore, confining such a material to length scales of nanometers is expected to change the properties of the liquid and to provide interesting information on the structure-dynamics relation in these complex systems. Although a tremendous amount of data on the nanoconfinement of supercooled liquids and polymers can be found in the literature, the understanding of the observed effects is far from being complete. In fact, a recent overview suggests that not even the sign of a glass-transition shift can be predicted for a certain experimental situation.[20]

Solvation dynamics experiments have been employed in order to gain further insight into the effects geometrical confinement has on the dynamics of liquids.[21–23] The triplet state variant of this optical technique is specifically designed to address the slow relaxation features of viscous liquids near their glass transition.[24] Monolithic porous glasses of pure silica are ideal confinement candidates for this technique, because these samples provide optical access to the liquid

imbibed into Vycor or GelSil type porous glasses. Because the progress of the relaxation is monitored in terms of a time dependent redshift of the emission energy of solute molecules, the amount of volume probed and the signal intensities do not affect the results directly. Furthermore, ambiguities resulting from dielectric mixing effects[25–27] remain absent in these experiments. In recent studies, we have used triplet state solvation techniques for focusing on the dynamics of a confined liquid at the liquid/solid interface,[28] and for comparing hard versus soft boundary conditions.[29]

In the present work, we elaborate on these methods with the aim of providing a more detailed understanding of the role of the interfacial effects relative to pure finite size effects. To this end, the dynamics of 3-methylpentane is measured in porous glasses with the chromophore attached to the pore wall. This approach to spatially resolved dynamics within a pore relies on nonpolar solvents, so that a polar chromophore is driven to bind to the silanol groups of the surface. The motivation to obtain such data for different pore sizes is to determine whether pore size and surface curvature have a significant impact on the behavior of the interfacial liquid layer. Experiments involving the glass-forming polyols, propylene glycol and glycerol, are meant to explore the differences in soft versus hard confinement. Because soft confinement is realized in terms of reverse micelles, these studies are currently limited to liquids as the water phase that are sufficiently polar to assure the absence of miscibility with the glass-forming oil phase decalin. These polyols are then measured in hard confinement by the same experimental technique in order to provide a direct comparison between soft and hard interfaces in the case of comparable spatial confinement.

II. EXPERIMENTS

In a solvation experiment, the liquid under study is doped at low concentrations with chromophores, i.e., molecules which can be excited selectively into a higher electronic level by the absorption of light.[30,31] In general, these solute molecules will exhibit a permanent dipole moment in the excited state (μ_E) which is different from that in the ground state (μ_G). Such a laser induced transition of the electronic state changes the electric field surrounding the chromophore and the dipoles within a polar liquid are no longer in equilibrium with the field of the probe molecule. In the case of long-lived excited triplet states, optical emission can be observed for times which are long compared with typical fluorescence lifetimes of several nanoseconds.[32] Analogous to a dielectric relaxation experiment, the solvent molecules in the immediate vicinity of the solute will tend to align in order to reestablish equilibrium with the excited state dipole of the probe.[33] In the absence of dipolar interactions, the effects are limited to the smaller responses of mechanical solvation, which originate from an excitation induced change in the pair potential or effective solute size.[34–36] For the present purpose, one of the important aspects of the solvation technique is the local probing of dynamics, which is spatially limited to approximately the first solvent shell or nearest neighbor molecules.

Solvation experiments record the time dependent emission spectra following electronic excitation of the chromophore in liquid solution, because the emission energy of the solute is a direct measure of the solvent response. Time dependent Stokes shifts of the mean emission energy can be observed, provided that the solvent reorganizes within the excited state lifetime of the probe. Accordingly, long lived $S_0 \leftarrow T_1$ (0-0) phosphorescence is required in order to study the slow dynamics of supercooled liquids near T_g.[24] Being interested in the solvent dynamics rather than absolute emission energies, it is usually sufficient to focus on the average transition energy in terms of $\overline{\nu}$, which is related to the Stokes shift correlation function $C(t)$ via normalization,[30]

$$C(t) = \frac{\langle \overline{\nu}(t) \rangle - \langle \overline{\nu}(\infty) \rangle}{\langle \overline{\nu}(0) \rangle - \langle \overline{\nu}(\infty) \rangle}. \quad (1)$$

Technical details of the experiments have been discussed previously.[24] An advantageous feature of the optical probing of local dielectric responses is the possibility of positioning the chromophores specifically where the solvent response is of interest.[28]

The porous glass samples used in this work are GelSil (GelTech) samples with nominal pore diameters of 5.0 nm and 7.5 nm, where the porous structure of the silica sample is a result of a sol-gel transition and further annealing. We have also employed Vycor (Corning) glasses with 4 nm pore diameter, manufactured by spinodal decomposition. Both types of porous glasses are sufficiently transparent at the laser wavelength of 308 nm and remained free of luminescence. The liquids used within these hard confinement samples are 3-methylpentane (3MP, Aldrich, 99+%), propylene glycol (PG, Aldrich, 99.5%, anhydrous), glycerol (GLY, Aldrich, 99.5%, anhydrous), and 2-methyltetrahydrofuran (MTHF, Aldrich, 99+%, purified by distillation). As chromophores we have used quinoxaline (QX, Aldrich, 98%, purified by sublimation) and naphthalene (NA, zone refined), both at a concentration around 5×10^{-4} mol/mol.

Our approach to measuring the dynamics specifically at the interface of a liquid confined to porous glass exploits the affinity of the chromophore QX to the silanol groups of a clean silica surface instead of remaining dissolved in a nonpolar solvent like 3MP.[23] For QX/3MP in 7.5 nm pores, the feasibility of this technique has been demonstrated in a previous publication.[28] At that time, the attempt to repeat the experiment in 5.0 nm pores failed repeatedly, because some additional spectrally broad phosphorescence emission masked the $S_0 \leftarrow T_1$ (0-0) transition of QX of interest. As a result of the present study, we assume that the smaller pore size promoted clustering of QX. The successful method of sample preparation is to introduce QX into the porous glass by a better solvent, e.g., MTHF. Then MTHF is evaporated, leaving the uniformly dispersed QX in the pores, and the sample is refilled with neat 3MP. The emission spectra of QX obtained in this way for the 5.0 nm pores are very similar to the previous 7.5 nm case, i.e., the additional emission that prevented the measurement is lacking.

The spatial position of QX in 3MP within porous glasses is clearly identified by the substantial shift of approximately

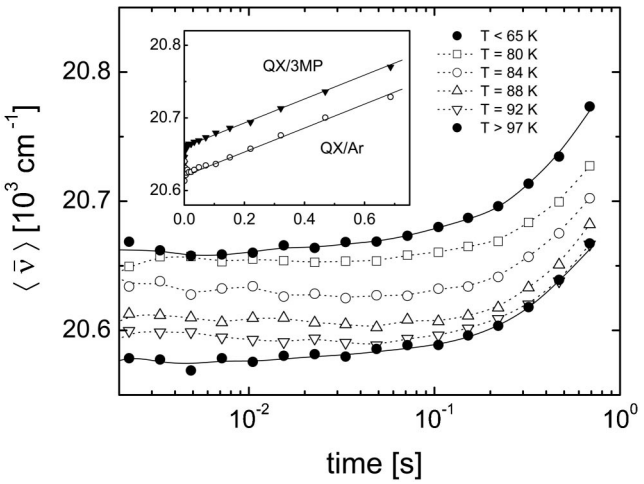

FIG. 1. Time resolved emission energies $\langle \overline{\nu} \rangle$ for QX/3MP in 7.5 nm pores, where QX is attached to the silanol groups of the silica pore walls. The temperature dependent solvation process superimposes onto a gradual blueshift with increasing time. The inset shows the linear behavior of this blueshift with time at $T=60$ K, $\langle \overline{\nu} \rangle = 20\,660\ \text{cm}^{-1} + 165\ \text{cm}^{-1} \times (t/\text{s})$, which persists even when 3MP is replaced by argon gas (QX/Ar, $T=102$ K). After subtracting the $165\ \text{cm}^{-1} \times (t/\text{s})$ feature, normal Stokes shift dynamics are obtained.

760 cm^{-1} towards lower energies compared with the bulk QX/3MP sample. For QX, such low emission energies are observed otherwise only if the chromophore is dissolved in alcohol. We therefore conclude that in the porous glasses QX attaches to the silanol-OH groups present on a clean silica surface.[28] An unexpected feature of the emission spectra in cases where QX is bound to the glass surface is a temperature invariant blueshift which is equally observed in all pore sizes and also in the absence of any solvent. This effect adds to the otherwise normal solvation redshift, and is therefore easily eliminated in terms of an appropriate data analysis. We assume that this blueshift is similar in origin to what has been observed in the system QX/3-bromopentane, where the excited state lifetime varies systematically within the emission band.[37] As a result, the intensities within the lower energy part of the emission band decay faster, thus leading to an apparent blueshift of the spectrum. The explanation for the energy-lifetime correlations rested upon the idea that a higher concentration of bromine at the solute generates a high polarizability and thus low emission energy, and it reduces the phosphorescence lifetime via the external heavy-atom effect. For the present case, both the redshift and the blueshift are displayed in Fig. 1 for the QX/3MP in 7.5 nm pores sample. That the blueshift does not originate from the solvent is shown by a comparison with the signal obtained after replacing the solvent with argon gas, which does not alter the blueshift feature (see inset of Fig. 1). In both cases, the apparent blueshift is linear in time with a slope of +165 cm^{-1} per second.

In order to realize soft confinement of dimensions comparable to the porous glass confinement, glass-forming microemulsions have been prepared from an intramicellar polar liquid or water phase, PG or GLY, a nonpolar oil phase or matrix decalin (DHN), and a surfactant AOT [sodium bis(2-ethylhexyl)sulfosuccinate, aerosol OT, Aldrich].[29] The surfactant AOT has been dried in a vacuum oven prior to use. For certain composition ranges, the reverse micelles obtained from these ternary mixtures remained stable upon cooling to the glass-transition temperature of the intramicellar material, $T_g \approx 168$ K for PG and $T_g \approx 188$ K for GLY. In this temperature range, the extramicellar phase decalin remains fluid, as its T_g is around 135 K.[38] The following microemulsions have been studied by solvation dynamics: 5.0% PG/ 39.0% AOT/ 56.0% DHN leading to 2.6 nm PG droplets, 10.2% PG/ 36.1% AOT/ 53.7% DHN leading to 4.6 nm PG droplets, and 12.0% GLY/ 31.2% AOT/ 56.8% DHN leading to 5.0 nm GLY droplets. The percentage values refer to weight fractions, the stated diameters $2R$ are estimated based on the volume fractions, on an AOT layer thickness of $r=1.33$ nm, and on spherical particles using the following equation:[39]

$$\frac{V_{\text{AOT}}}{V_{\text{PG}}} = \frac{\frac{4}{3}\pi[(R+r)^3 - R^3]}{\frac{4}{3}\pi R^3} = \left(1 + \frac{r}{R}\right)^3 - 1. \qquad (2)$$

The phase diagrams for stable microemulsions at 298 K and 77 K are shown in Fig. 2 for PG (a) and for GLY (b), also indicating the particular compositions studied by solvation dynamics in terms of solid symbols.

III. RESULTS

Regarding the dynamics of confined and interfacial 3MP, the main objective was to study the 5.0 nm nominal pore size sample for a comparison with the results obtained for the larger diameter and to obtain more data on the dynamics as a function of the average distance from the pore wall. The emission spectra of QX bound to the pore wall are recorded as a function of time and temperature. From these Gaussian profiles, the average energies are derived, leading to raw solvation dynamics data such as the example shown in Fig. 1. The solvent response is best extracted from such data by normalizing according to Eq. (1) and subjecting the resulting $C(t)$ curves to suitable relaxation functions. In the case of viscous liquids, $C(t)$ decays deviate significantly from simple exponential patterns.[40] Fitting the relaxation of supercooled systems can be achieved by stretched exponential or Kohlrausch-Williams-Watts (KWW) functions,

$$C(t) = \exp\left[-\left(\frac{t}{\tau_0}\right)^{\beta}\right]. \qquad (3)$$

Such a fit quantifies the characteristic relaxation time scale by τ_0 and the degree of nonexponentiality by the exponent β. Within the limited experimental temperature ranges, the stretching exponents β do not change significantly with temperature. As typical for supercooled liquids, the characteristic time scales of the dynamics depend on temperature according to the Vogel-Fulcher-Tammann (VFT) law,

$$\log_{10}(\tau_0/s) = A + B/(T - T_0). \qquad (4)$$

The dynamics of interfacial 3MP in pores of 5.0 nm diameter is characterized by a stretching exponent $\beta=0.25$, and a temperature dependent time scale $\tau_0(T)$ that follows a VFT behavior with $A=-13.5$, $B=464$ K, and $T_0=52$ K. The activa-

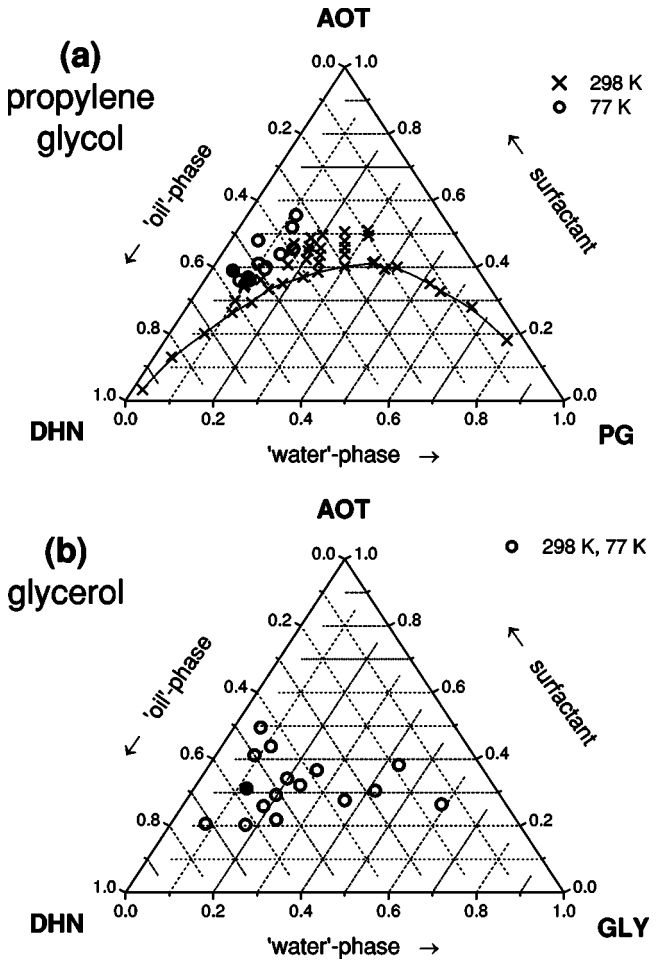

FIG. 2. (a) Composition phase diagram for the ternary systems propylene glycol (PG), AOT, decalin (DHN), identifying stable microemulsions at 298 K by crosses and those that are also stable at 77 K by circles. Phase boundaries are from Ref. 29. Solid sybols refer to compositions used for measuring solvation dynamics in reverse micelles. (b) Analogous graph for glycerol (GLY), AOT, decalin (DHN), where all compositions shown remained stable at 77 K.

tion map for this result is shown in Fig. 3. The total redshift for this QX/3MP in 5 nm pore sample is $\Delta\overline{\nu}=74$ cm^{-1}. Additional solvation results for confined 3MP are obtained using naphthalene as chromophore, which remains dissolved in 3MP and is thus expected to sample the pore volume average. In this case Vycor glass with a pore diameter of 4 nm has been used, for which the average distance of the probe molecules from the surface is 0.5 nm (see below). The resulting dynamics of 3MP in pores of 4.0 nm diameter displays an exponent $\beta=0.20$, and a temperature dependent relaxation time $\tau_0(T)$ that is well described by a VFT law with $A=-14.1$, $B=464$ K, and $T_0=52$ K, as shown in Fig. 3. A previous measurement of a NA/3MP sample in 4 nm Vycor pores deviates from the current results because the sample had not been equilibrated sufficiently.[41]

In the remainder of this section, the results related to the soft confinement by glass-forming microemulsions are described. The two liquids studied here are PG and GLY, both highly polar glass-forming polyalcohols. The solvation dy-

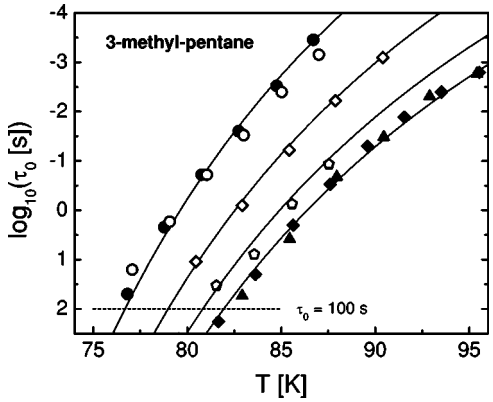

FIG. 3. Temperature dependence of the solvent relaxation time τ_0 in 3-methylpentane (3MP) for the bulk liquid (QX/3MP, solid circles; NA/3MP, open circles), for confinement to 7.5 nm pores (NA/3MP, open diamonds), for confinement to 4.0 nm pores (NA/3MP, open pentagons), and for the interfacial layer of 3MP at the pore wall (QX/3MP in 7.5 nm, solid diamonds; QX/3MP in 5.0 nm, solid triangles). Data for 7.5 nm pores are from Ref. 28. The solid lines are VFT curves with $B=464$ K, $T_0=52$ K, and $A=-16.8$, -15.2, -14.1, and -13.5, in the order from top to bottom curve.

namics based upon QX as a probe in the bulk liquids are indicative of this high polarity, yielding $\Delta\overline{\nu}=515$ cm^{-1} for PG and $\Delta\overline{\nu}=588$ cm^{-1} for GLY. The Stokes-shift correlation functions $C(t)$ are very nonexponential relative to the dielectric counterparts,[42] with the KWW exponents being as low as $\beta=0.37$ for PG and $\beta=0.38$ for GLY. The temperature dependence for the solvent response times in the bulk situation closely resembles the curves obtained from dielectric relaxation data. The activation behavior, $\tau_0(T)$, derived from the $C(t)$ results for PG and GLY are depicted in Figs. 4 and 5, respectively. For the two liquids, both hard and soft confinement has been realized in terms of porous Vycor glass (4 nm diameter) and AOT/DHN type microemulsions, respectively. The solvation times obtained under these condi-

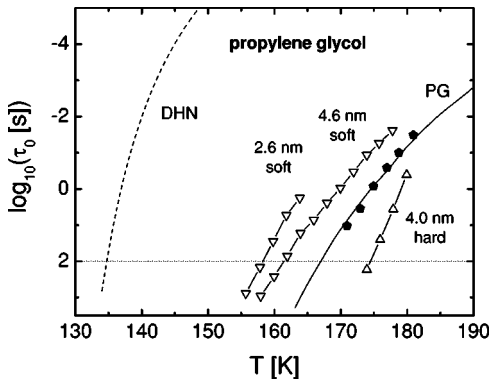

FIG. 4. Temperature dependent Stokes shift correlation times τ_0 obtained from QX in PG for various confinement situations: bulk liquid (solid circles), in 4.0 nm diameter porous Vycor glass (triangles pointing up), and in 4.6 and 2.6 nm diameter droplets of PG/AOT/DHN microemulsions (triangles pointing down). Data for the 4.6 nm sample are from Ref. 29. The solid line indicates the dielectric relaxation trace for bulk PG, the dashed curve is for the dielectric result for bulk DHN, taken from Ref. 38. The dotted horizontal line represents the $\tau_g=100$ s criterion for identifying T_g.

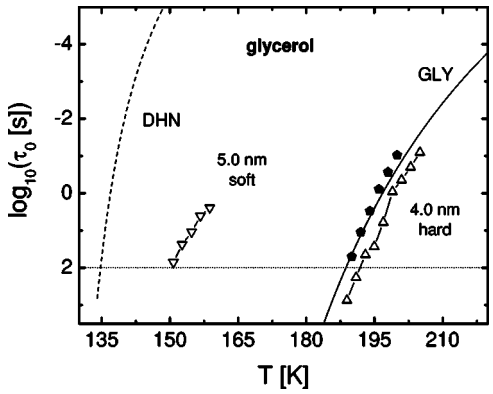

FIG. 5. Temperature dependent Stokes shift correlation times τ_0 obtained from QX in GLY for various confinement situations, bulk liquid (solid circles), in 4.0 nm diameter porous Vycor glass (triangles pointing up), and in 5.0 nm diameter droplets of GLY/AOT/DHN microemulsions (triangles pointing down). The solid line indicates the dielectric relaxation trace for bulk GLY, the dashed curve is for the dielectric result for bulk DHN, taken from Ref. 38. The dotted horizontal line represents the $\tau_g = 100$ s criterion for identifying T_g.

tions are included in the graphs of Figs. 4 and 5. Some relevant values related to the relaxation behavior are compiled in Table I.

TABLE I. Relaxation parameters for the liquids PG and GLY subject to different confinement conditions, KWW stretching exponent β and glass transition temperature T_g. The value of T_g is based upon the criterion $\tau_g = \tau(T_g) = 100$ s.

Liquid		Confinement	Size	β	T_g/K
Propylene glycol	(PG)	Bulk	∞	0.37	168
		Hard	4 nm	0.20	174
		Soft	2.6 nm	0.25	158
		Soft	4.6 nm	0.25	161
Glycerol	(GLY)	Bulk	∞	0.38	188
		Hard	4 nm	0.20	192
		Soft	5 nm	0.36	151

IV. DISCUSSION

Experimental approaches to the behavior of confined and interfacial liquids have used very different techniques,[3–5,7,43–48] confining geometries,[2,49–52] and surface properties[8,22,53]. An attempt to sort the various experimental approaches to confined liquids by the confinement type is shown in Table II, which disregards surface treatments as an additional experimental variable. Due to this diversity, it is not surprising, that the observations do not follow a universal trend.[20] For supercooled materials, the effect of confinement has often been reported in terms of a glass transition shift. Casting the effects of a restricted geometry into a single value, ΔT_g, implies that the shape of the correlation function and the amplitude of the relaxation process did not change appreciably. However, significant changes in the relaxation time dispersion[29,54] and even the appearance of bimodal relaxations[22,55] are common. If the confinement gives rise to a bimodal relaxation scenario, the quantity ΔT_g is quite meaningless. Therefore, a glass transition shift must be interpreted with the appropriate caution.

There is an important reason why the relaxation amplitude deserves the same attention as does the average relaxation time when comparing relaxations for confined and bulk samples.[56] Consider a nonexponential relaxation process for the bulk situation of some material, e.g., a KWW type correlation decay with $\beta = 0.5$. Such a case is represented by the solid curve in Fig. 6 in terms of the probability density. Two different scenarios are considered as confinement effects. The effect of confining this system is to freeze much of the slower relaxation contributions, such that their relaxation is too slow to be observed. Then only the faster components remain visible within the experimental window of observation, as indicated by the 30% fast modes shown as short-dashed curve in Fig. 6. A very different effect of confinement would be a uniform shift of all relaxation modes towards faster time scales, represented by the dashed curve in Fig. 6. If the amplitudes are disregarded, the two dashed curve would both be interpreted as an acceleration of the dynamics by a common factor of 10, if judged on the basis of the peak position of $g(\ln \tau)$. Therefore, knowledge of the response amplitudes are required in order to discriminate the very different sources of apparently shifting the most probable relaxation time towards smaller values of τ. While Fig. 6 outlines these distinct situations in terms of the probability density of relaxation times, the analogous consequences for a time-domain correlation function and for frequency domain susceptibility data have been shown elsewhere.[56]

Solvation dynamics experiments on confined liquids are advantageous because—unlike other technique—the response amplitude is independent of the amount of chromophores and volume probed. In previous studies it has been shown in detail that ≈95% of the bulk amplitude is recovered in a triplet state solvation experiment on liquids confined to pores of 5 nm diameter.[41,57] In the present experiments, the relatively high temperature and concomitant fast oxygen diffusion prohibit identifying the amplitudes unambiguously. While only part of the amplitudes (30%–75%) are seen in some cases, the KWW fits to $C(t)$ data suggest that the values of $\Delta\overline{\nu}$ are practically unchanged in the case of the confined systems relative to the bulk. In any case, the faster dynamics presently observed in microemulsion confinement cannot be explained by the freezing of slower components in the way outlined in Fig. 6.

We begin the discussion of the present results by focusing on the solvation dynamics of 3-methylpentane (3MP) in various hard confinement and interfacial situations. Adding data obtained for 4 nm and 5 nm pore sizes to the larger 7.5 nm pore diameter case[28] provides important information. The first result originates from the chromophore QX positioned at the interface of 7.5 nm and 5.0 nm GelSil porous glasses. As shown in Fig. 3, the dynamics is slower by a common factor of 2000 relative to the bulk for the two pore sizes. Both the pore volume averaged dynamics (factor of ≈10, see below) and the surface curvature (factor of 1.5) differ for the pore

TABLE II. Compilation of different confinement and interfacial conditions for which dynamics have been studied. In some cases, the surface chemistry is an additional variable.

Dimensionality	Hard confinement	Soft confinement
One dimensional	Substrate supported films	Free surface thin films
	Single surfaces (sapphire)	
	Layers (clay, mica)	
Two dimensional	MCM-41, SBA-15	
	Anodisc channels	
Three dimensional	Zeolites	Microemulsions
Regular	Silicalites	Polymer sphere suspension
Three dimensional	Porous glasses	
Irregular	Glass beads, sand, rocks	
	Polymer solutions	

sizes 7.5 and 5.0 nm, but with no detectable effect on the interfacial solvent response. Therefore, proximity to the surface appears to be the main factor in determining this drastic reduction in molecular mobility at the 3MP/silica interface.

Using NA instead of QX in confined 3MP eliminates the preferential positioning of the probe molecules at the surface and the pore volume average rather than surface specific features are being measured. Both samples studied via the solvation of NA, 4.0 nm Vycor and 7.5 nm diameter GelSil (Ref. 28) samples, display increased relaxation times compared with the bulk, albeit not as pronounced as the interfacial situation. The relative dynamic frustration in terms of the relaxation time ratio $\tau_0/\tau_{\text{bulk}}$ is 500 for the 4 nm pore size and 40 for 7.5 nm diameter. Based upon spherical geometries, these diameters translate into average particle distances $\langle x\rangle = R/4$ from the interface of 0.5 nm and 0.94 nm, respectively.[28] It is important to realize that these two values are less than the typical lengths scales identified with the cooperative nature of dynamics in such viscous liquids. The length ξ associated with cooperativity can be understood as the minimum distance required for two molecules to relax independently, with values for ξ claimed to be of order 3 ± 2 nm.[22,56,58,59] Unless the cooperative character in supercooled liquids changes significantly upon confinement, we do not expect that the molecules in these pores relax independently of the strongly frustrated condition which exists at the interface. In fact, we consider cooperativity all that is required to explain the pore size dependence without invoking any further finite size effects. On a similar premise, cooperativity length scales have been determined for model glass formers by Donati and Jäckle.[60] For the given interfacial situation characterized by $\tau_0 = 2000 \times \tau_{\text{bulk}}$, we attempt to explain the effect of confinement by the idea that the length scale ξ of cooperativity determines the extent to which the interfacial frustration penetrates into the pore volume. This picture emphasizes interfacial over true finite size effects, but without claiming a dynamically distinct and well separated interfacial layer which differs qualitatively from the remaining liquid.

For a more quantitative treatment of confinement effects in terms of an interfacial modification of the dynamics combined with cooperativity, we write the bulk dynamics as a superposition of exponential contributions in order to define the probability density $g(\tau/\tau_0)$ of relative relaxation times for a given bulk correlation function $C_{\text{bulk}}(t)$,

$$C_{\text{bulk}}(t) = \int_0^\infty g(\tau/\tau_0) e^{-t/\tau} d\tau. \tag{5}$$

The reference value τ_0 can be any characteristic time constant, like the average or most probable value of τ. We now assume a gradient of the characteristic relaxation time normal to the liquid/solid interface, i.e., a τ_0 that (on average) changes with the distance from the interface. For the present example of 3MP, the dynamics at the interface and those at different average distances from the interface provide an idea of what the intrapore gradient could look like.[29] A graphical compilation of the relaxation times as a function of average distance x relative to the bulk case is shown in Fig. 7, along with an exponential fit $\log_{10}(\tau_0/\tau_{\text{bulk}}) = 3.6$

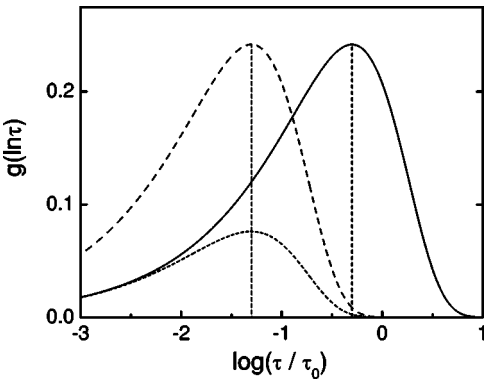

FIG. 6. Calculated probability density $g(\ln\tau)$ of logarithmic relaxation times $\ln\tau$ for a KWW type relaxation function with $\beta = 0.5$ (solid line). There are two distinct ways of generating a peak at shorter time scales: by shifting the entire curve by one decade while preserving its amplitude (dashed line), or by freezing 70% of the slowest contributions, leaving the faster 30% with concomitantly reduced amplitude (short dashed line). This shows that the amplitude is important for discriminating a uniform acceleration of the dynamics from the complete arrest of the slower relaxation modes.

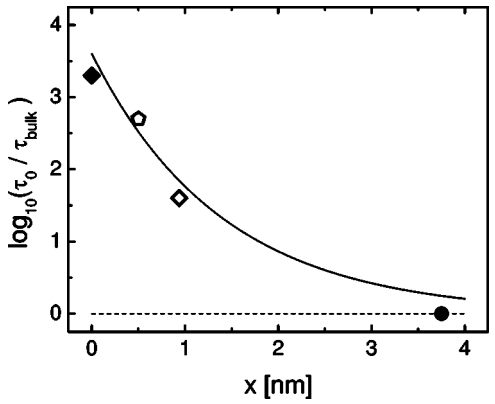

FIG. 7. Characterisic relaxation times relative to the bulk case, $\tau_0/\tau_{\mathrm{bulk}}$, shown for different average distances x from the pore wall. The symbols (same as Fig. 3) refer to different confinement situations: in 7.5 nm pores ($x=0.9$ nm), in 4.0 nm pores ($x=0.5$ nm), and for the interfacial layer of 3MP at the pore wall ($x\approx 0$). The bulk symbol is placed at $x=3.75$ nm, the center of a 7.5 nm pore, instead of its actual $x\rightarrow\infty$ limit (see text). The line represents the function $\log_{10}(\tau_0/\tau_{\mathrm{bulk}})=3.6\times\exp(-x/1.4\ \mathrm{nm})$.

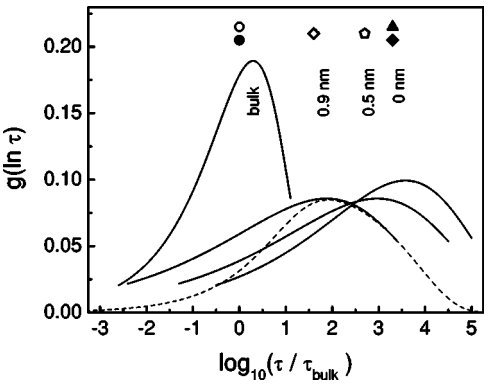

FIG. 8. Probability densities $g(\ln\tau)$ for the solvation dynamics in 3-methylpentane for a temperature of $T=81.4$ K, equivalent to $\tau_0=1$ s for the bulk liquid. In the order of increasing peak relaxation time, the curves are for the bulk liquid ($\tau_0=1$ s), for confinement to 7.5 nm pores ($\tau_0=40$ s), for confinement to 4.0 nm pores ($\tau_0=500$ s), and for the interfacial layer of 3MP at the pore wall ($\tau_0=2000$ s). The curves for $g(\ln\tau)$ are displayed only in the τ ranges which are relevant for the $0.15\leqslant C(t)\leqslant 0.85$ interval. The symbols correspond to those used in Fig. 3, positioned at their respective τ_0 values.

$\times\exp(-x/1.4\ \mathrm{nm})$ which quantifies the distance dependence $\tau_0(x)$. The reason for placing the symbol for the bulk case, $\log_{10}(\tau_0/\tau_{\mathrm{bulk}})=0$, at $x=7.5\ \mathrm{nm}/2$ originates from the observation that the relaxation time distributions for the bulk and 7.5 nm pore cases merge for short times (see Fig. 8).[28] Note that a picture similar to Fig. 7 has been derived from a confined binary Lennard-Jones model of a liquid by Scheidler *et al.*, also displaying a gradual change in relaxation time by three orders of magnitude as the surface is approached.[61] The remaining information required is the probability density $p(x)$ of finding a particle at a certain distance x away from the interface. Approximating the pores by spherical geometries with pore radius R, $p(x)$ is readily calculated as $p(x)=3(R-x)^2/R^3$. In the absence of other effects, this model predicts

$$C(t)=\int_0^{\infty}\left(\int_0^{x_{\max}}p(x)g[\tau/\tau_0(x)]dx\right)e^{-t/\tau}d\tau, \qquad (6a)$$

or

$$\text{or}\quad C(t)=\int_0^{x_{\max}}p(x)\exp\{-[t/\tau_0(x)]^{\beta}\}dx. \qquad (6b)$$

In Eq. (6a), it is assumed that the only effect of distance x is to alter the characteristic time τ_0, which shifts the distribution of relaxation times along the $\ln\tau$ scale without changing its shape. The expression within the large parentheses in Eq. (6a) can be considered the volume averaged probability density $g_{\mathrm{conf}}(\tau)$ for the confined liquid. The same behavior can be expressed by Eq. (6b) in terms of a spatial average over KWW type relaxation functions with constant exponent β but position dependent τ_0. Equation (6b) is obtained from Eq. (6a) after changing the order of integration and assuming a KWW type density $g(\tau/\tau_0)$ that leads to $C_{\mathrm{bulk}}(t)=\exp[-(t/\tau_0)^{\beta}]$. Two features are inherent in the present approach: more nonexponential dynamics compared with the bulk, and a trivial dependence on pore size. The increased width of the relaxation time distribution stems from the additional dispersion of having a relaxation time gradient quantified by $\tau_0(x)$. The pore size enters this picture only in terms of the distribution of distances from the interface, as gauged by $p(x)$ and $x_{\max}$, without involving any other finite size effects.

In order to compare the relaxation time distributions for the experimental situations realized for 3MP, we have fitted the generalized gamma probability density $g_{\mathrm{GG}}(\tau)$ to the KWW correlation functions $C(t)$, with

$$g_{\mathrm{GG}}(\tau)=\frac{\gamma}{\tau\Gamma(\alpha)}\left(\frac{\tau}{\tau_{\mathrm{GG}}}\right)^{\alpha\gamma}\exp\left[-\left(\frac{\tau}{\tau_{\mathrm{GG}}}\right)^{\gamma}\right]. \qquad (7)$$

This distribution is known to approximate KWW behavior quite accurately for stretching exponents $\beta<0.6$,[62] while circumventing the numerical problems inherent in the true KWW probability density.[63] The curves for bulk ($\beta=0.42$), confined ($\beta=0.22$ for 7.5 and 4.0 nm), and interfacial ($\beta=0.25$) 3MP are shown in Fig. 8 as solid lines. As observed in many experiments, the relaxation of the confined liquid displays a more pronounced dispersion (lower β) compared with the bulk counterpart. This excess broadening of the relaxation time dispersion is in accord with the above model. However, the interfacial relaxation is almost as disperse, presumably caused by distributions of surface roughnesses and probe orientations. According to the steepness of the $\tau_0(x)$ curve at small values of x, subtle variations of the effective distance will give rise to a considerable broadening near the interface. Although such effects remain disregarded by the approach of Eq. (6), the relaxation dispersion of confinement to 7.5 nm pores is approximately reproduced by the dashed curve in Fig. 8, which is obtained using Eq. (6a) for a probability density $g(\tau/\tau_0)$ equivalent to the bulk exponent of β

$=0.42$, a spatial variation of the dynamics $\tau_0(x)$ as shown in Fig. 7, and for spherical pores with $R=3.75$ nm. Although not in quantitative agreement, much of the excess width near the peak relative to the bulk curve is accounted for by this simple approach.

The above approach to dynamics in confined liquids clearly emphasizes interfacial effects while disregarding true finite size effects, like those considered elsewhere[64] for the marginal glass-former toluene in MCM-41 and SBA-15 matrices with highly regular geometries. In the present study, confinement dimensionality changes necessarily along with the transition from soft to hard interfacial conditions. Therefore, alternative models which invoke a shift from interfacial to finite size effects upon changing the confinement dimensionality from two dimensional (2D) to three dimensional (3D) may be considered as well. Within the present view of surface effects dominating the dynamics in confinement, altering the conditions at the interface should result in different dynamics, even if the spatial dimensions of the confinement remain the same. A triplet state solvation study of viscous 2-methyltetrahydrofuran has demonstrated exactly this effect by focusing on the effects of altering the surface chemistry from hydrophilic to hydrophobic.[22] A more extreme case of altering the interfacial situation is to change from hard to soft confinement. These terms are meant to specify the dynamics of the confining matrix relative to the confined material under study. Hard confinement refers to cases, like porous glasses, where the matrix that defines the geometry exhibits slower dynamics or increased viscosities relative to the liquid inside the pore. Porous glass is an extreme case of hard confinement, in which the matrix is static on all experimental time scales. The two glass-forming liquids addressed below, propylene glycol and glycerol, have both been subject to dielectric investigations in confined spaces. For PG, an increase of the relaxation time τ and (equivalently) glass transition temperature T_g has been reported in a number of studies,[43,45,53,65,66] consistent with our solvation result in 4 nm Vycor glass. Only one study reports the reverse effect of faster dynamics upon hard confinement.[67] Also consistent with previous dielectric findings[68] is our present observation that the hard confinement to porous glass has a relatively small impact in the case of GLY.

Sample boundaries that represent virtually free surfaces have been achieved in the case of polymeric materials as self-supporting films[12,13] or suspended spheres.[69] In the case of molecular systems, similarly soft confinement is one we have realized earlier in terms of glass forming microemulsions,[70,71] with droplets of viscous propylene glycol being suspended in the much more fluid decalin, where AOT acts as surfactant.[29] The case of PG measured by solvation dynamics in hard (4 nm Vycor) and soft confinement (droplets of 2.6 and 4.6 nm diameter) is shown in Fig. 4 and provides a direct comparison of different dynamical properties of the confining matrix for similar spatial dimensions of the restricting geometries. While the relaxation of PG in porous glass is slower than the bulk PG just as in the 3MP case discussed above, confinement to similar and even smaller droplet diameters reverses the effect from frustration to acceleration. In the case of PG, confinement leaves the relaxation amplitudes practically unchanged and no indications of bimodal relaxation behavior is observed. Therefore, the effect of confinement can be summarized by hard versus soft boundary conditions changing the glass transition temperature T_g from above ($\Delta T_g=+6$ K) to below ($\Delta T_g=-7$ K) the bulk value of $T_g=168$ K. According to Fig. 5, the confinement induced changes of T_g are qualitatively similar in the case of GLY, but the magnitudes of the effects differ strongly for hard and soft surfaces.

Relative to the bulk, the relaxation patterns in the nanodroplets display smaller values of the stretching exponents β, equivalent to wider relaxation time distributions. This increased dispersion and the dependence of the extent of the confinement effect on the droplet size are qualitatively similar to the features seen in the cases of hard confinement. Therefore, we believe that a similar gradual approach to bulk like dynamics will occur in the reverse micelles as the distance from the surfactant is increased towards the center of the droplet. Accordingly, a picture analogous to Fig. 7 but with inverted ordinate scale is expected, with the penetration depth of $\xi=1.4$ nm for 3MP being replaced by the concomitant value for PG (for which a value of <1 nm has been noted by Gorbatschow *et al.*[66]). Because of the presence of the surfactant, accelerated dynamics based upon the fluidity of the DHN matrix in these reverse micelles is not entirely trivial. The size and molecular weight of AOT is significantly larger than the respective DHN values, which leads to expecting slower dynamics within the surfactant layer compared with DHN.[72] On the other hand, vibrational energy relaxation across the AOT layer is found to be very effective.[73] At present, the mechanism by which extramicellar and intramicellar dynamics interact through the AOT layer remains unclear.

As a result of emphasizing interfacial over finite size effects in our present approach, analogous effects are expected in the immediate vicinity of a single planar surface which is in contact with a liquid of otherwise unrestricted geometry. The small surface to volume ratio of such a sample prohibits the observation of interfacial dynamics for most experimental approaches. However, solvation dynamics combined with surface specific excitation via total internal reflection has been demostrated to overcome this problem in the case of fluorescent probes.[74] This and many other examples of confinement effects on the nanosecond (or faster) dynamics of liquids clearly show that drastic changes of the relaxation time at the interface such as those observed here are restricted to the cases of surpercooled liquids.[75] In the fluid regime characterized by ps to ns time scales, the frustration at the liquid/solid interface rarely exceeds a factor of 3 in terms of the relaxation time increase over the bulk value.[76] The spatial extent of modified surface dynamics is a monolayer or smaller, according to a Kerr effect study on CS_2 across a wide range of temperatures.[77] We assume that the limited spatial range of the effect and the more moderate changes in the relaxation times are both a consequence of the much reduced length scale of cooperative effects at the higher temperatures, where ξ is not expected to exceed the dimensions of a molecule significantly.[78]

A possible qualitative approach to the pronounced interfacial effects observed for very viscous materials is as follows: In the absence of specific interactions between the liq-

uid under study (e.g., alkanes) and the surface, the increase of the hydrodynamic volume through steric hindrance is a straightforward explanation of an additional barrier to rotation over the bulk case.[79] For dynamics as fast as several picoseconds, this model explains the increase in reorietation time by a factor of approximately 2 at the surface. In the case of a viscous liquid, this additional interfacial barrier to rotation could be multiplied by the number of cooperatively relaxing molecules that are in contact with the interface, leading to the much more pronounced changes of the dynamics seen for supercooled liquids near their glass transition.

V. SUMMARY AND CONCLUSIONS

Triplet state solvation dynamics experiments have been employed in order to investigate the effects of spatial confinement and interfaces on the dynamics of supercooled liquids in their viscous regime. The length scales of the geometrical restrictions studied here range from 2.6 to 7.5 nm, with the emphasis on the effects of hard versus soft interfaces. The first part focuses on the nonpolar glass-former 3-methylpentane in porous silica glasses, for which no specific interactions with the surface are expected. Probing the interfacial dynamics with chromophores that are attached to the pore surface reveals that the surface layer of 3MP is a factor of 2000 slower than the bulk liquid at the same temperature. Interestingly, this pronounced frustration of the relaxation is independent of the pore size, 5.0 vs 7.5 nm, although the pore volume averaged relaxation time differs by a factor of ≈ 10 for these two diameters. From comparing interfacial relaxation time with the pore volume averages and the bulk behavior, we conclude that the interfacial effects dominate the confinement effects, with the cooperativity length scale ξ determining the spatial extent to which the interfacial behavior penetrates into the liquids. For 3MP near a slica surface, we find that the relaxation time gradient is well described by $\log_{10}(\tau_0/\tau_{\text{bulk}}) = 3.6 \times \exp(-x/1.4\ \text{nm})$, where x is the distance from the surface. This reduces the effect of pore size to the trivial geometric change of the distribution of distances of the molecules from the surface. The observation of a pronounced gradient of relaxation times (more than one order of magnitude across 1 nm) also implies that the confined liquid exhibits a larger relaxation time dispersion (smaller value of the stretching exponent β) compared with the bulk. The second part of our study focuses on exploring the effects of soft versus hard interfaces for comparable confinement geometries, again around diameters of a few nanometers. For two hydrogen-bonding glass-formers, propylene glycol and glycerol, the results are qualitatively similar. While hard confinement to porous glasses shifts T_g to higher values (equivalent to an increase of the relaxation time), confinement within a more fluid matrix results in negative T_g shifts. The important aspect of the reverse micelles in these glass-forming microemulsions is the lower glass transition (higher fluidity) of the extramicellar liquid (decalin) compared with the intramicellar nanodroplets of PG or GLY. Future variations of the intramicellar and extramicellar viscosities might elucidate the role of the surfactant AOT on the dynamics. Although soft confinement results in accelerated instead of frustrated dynamics, there is a analogous droplet size dependence. We interpret these microemulsion results as yet another indication of the interfacial situation being the decisive factor, whereas other finite size effects remain small or absent.

ACKNOWLEDGMENT

This material is based upon work supported by the National Science Foundation under Grant No. DMR 0304640 (NIRT).

[1] *Molecular Dynamics in Restricted Geometries*, edited by J. M. Drake and J. Klafter (Wiley, New York, 1989).
[2] G. Dosseh, Y. Xia, and C. Alba-Simionesco, J. Phys. Chem. B **107**, 6445 (2003).
[3] J. Zhang, G. Liu, and J. Jonas, J. Phys. Chem. **96**, 3478 (1992).
[4] J. Van Alsten and S. Granick, Phys. Rev. Lett. **61**, 2570 (1988); S. Granick, Science **253**, 1374 (1991).
[5] R. G. Horn and J. N. Israelachvili, J. Chem. Phys. **75**, 1400 (1981); J. N. Israelachvili and P. M. McGuiggan, Science **241**, 795 (1988).
[6] T. Becker and F. Mugele, Phys. Rev. Lett. **91**, 166104 (2003).
[7] D. D. Awschalom and J. Warnock, Phys. Rev. B **35**, 6779 (1987).
[8] J. M. Drake and J. Klafter, Phys. Today **43**, 46 (1990).
[9] M. D. Ediger, C. A. Angell, and S. R. Nagel, J. Phys. Chem. **100**, 13200 (1996).
[10] A. Patkowski, T. Ruths, and E. W. Fischer, Phys. Rev. E **67**, 021501 (2003).
[11] C. L. Jackson and G. B. McKenna, J. Non-Cryst. Solids **131–133**, 221 (1991).
[12] J. A. Forrest, K. Dalnoki-Veress, J. R. Stevens, and J. R. Dutcher, Phys. Rev. Lett. **77**, 2002 (1996).
[13] C. J. Ellison and J. M. Torkelson, Nat. Mater. **2**, 695 (2003).
[14] T. R. Böhme and J. J. de Pablo, J. Chem. Phys. **116**, 9939 (2002).
[15] C. A. Angell, K. L. Ngai, G. B. McKenna, P. F. McMillan, and S. W. Martin, J. Appl. Phys. **88**, 3113 (2000).
[16] G. Adam and J. H. Gibbs, J. Chem. Phys. **43**, 139 (1965).
[17] K. Schmidt-Rohr and H. W. Spiess, Phys. Rev. Lett. **66**, 3020 (1991).
[18] M. D. Ediger, Annu. Rev. Phys. Chem. **51**, 99 (2000).
[19] R. Richert, J. Phys.: Condens. Matter **14**, R703 (2002).
[20] G. B. McKenna, J. Phys. IV **10**, Pr7-53 (2000).
[21] D. M. Willard, R. E. Riter, and N. E. Levinger, J. Am. Chem. Soc. **120**, 4151 (1998).
[22] C. Streck, Yu. B. Mel'nichenko, and R. Richert, Phys. Rev. B **53**, 5341 (1996).
[23] H. Wendt and R. Richert, J. Phys.: Condens. Matter **11**, A199 (1999).
[24] R. Richert, J. Chem. Phys. **113**, 8404 (2000).
[25] R. Hilfer, Phys. Rev. B **44**, 60 (1991).
[26] X. Yan, C. Streck, and R. Richert, Mater. Res. Soc. Symp. Proc.

464, 33 (1997).
[27] R. Pelster, Phys. Rev. B **59**, 9214 (1999).
[28] R. Richert and M. Yang, J. Phys. Chem. B **107**, 895 (2003).
[29] L.-M. Wang, F. He, and R. Richert, Phys. Rev. Lett. **92**, 095701 (2004).
[30] M. Maroncelli and G. R. Fleming, J. Chem. Phys. **86**, 6221 (1987).
[31] G. R. Fleming and M. Cho, Annu. Rev. Phys. Chem. **47**, 109 (1996).
[32] R. Richert, F. Stickel, R. S. Fee, and M. Maroncelli, Chem. Phys. Lett. **229**, 302 (1994).
[33] R. Richert and A. Wagener, J. Phys. Chem. **95**, 10115 (1991).
[34] J. T. Fourkas, A. Benigno, and M. Berg, J. Non-Cryst. Solids **172–174**, 234 (1994).
[35] H. Wendt and R. Richert, J. Phys. Chem. A **102**, 5775 (1998).
[36] J. Ma, D. Vanden Bout, and M. Berg, J. Chem. Phys. **103**, 9146 (1995).
[37] A. Wagener and R. Richert, Chem. Phys. Lett. **176**, 329 (1991).
[38] K. Duvvuri and R. Richert, J. Chem. Phys. **117**, 4414 (2002).
[39] M. Kotlarchyk, S.-H. Chen, J. S. Huang, and M. W. Kim, Phys. Rev. Lett. **53**, 941 (1984).
[40] H. Wendt and R. Richert, Phys. Rev. E **61**, 1722 (2000).
[41] R. Richert and M. Yang, J. Phys.: Condens. Matter **15**, S1041 (2003).
[42] R. Böhmer, K. L. Ngai, C. A. Angell, and D. J. Plazek, J. Chem. Phys. **99**, 4201 (1993).
[43] G. Carini, V. Crupi, G. D'Angelo, D. Majolino, P. Migliardo, and Yu. B. Mel'nichenko, J. Chem. Phys. **107**, 2292 (1997).
[44] M. D'Angelo, D. Fioretto, G. Onori, and A. Santucci, Phys. Rev. E **58**, 7657 (1998).
[45] Yu. B. Mel'nichenko, J. Schüller, R. Richert, B. Ewen, and C.-K. Loong, J. Chem. Phys. **103**, 2016 (1995).
[46] Y. Ryabov, A. Gutina, V. Arkhipov, and Y. Feldman, J. Phys. Chem. B **105**, 1845 (2001).
[47] J. Schüller, R. Richert, and E. W. Fischer, Phys. Rev. B **52**, 15232 (1995).
[48] R. M. Dickson, D. J. Norris, Y.-L. Tzeng, and W. E. Moerner, Science **274**, 966 (1996).
[49] A. Huwe, F. Kremer, P. Behrens, and W. Schwieger, Phys. Rev. Lett. **82**, 2338 (1999).
[50] C. Svanberg, R. Bergman, P. Jacobsson, and L. Börjesson, Phys. Rev. B **66**, 054304 (2002).
[51] R. Bergman, J. Swenson, L. Börjesson, and P. Jacobsson, J. Chem. Phys. **113**, 357 (2000).
[52] G. Barut, P. Pissis, R. Pelster, and G. Nimtz, Phys. Rev. Lett. **80**, 3543 (1998).
[53] A. Huwe, M. Arndt, F. Kremer, C. Haggenmüller, and P. Behrens, J. Chem. Phys. **107**, 9699 (1997).
[54] D. Morineau, Y. Xia, and C. Alba-Simionesco, J. Chem. Phys. **117**, 8966 (2002).
[55] B. J. Loughnane, R. A. Farrer, and J. T. Fourkas, J. Phys. Chem. B **102**, 5409 (1998).
[56] R. Richert, Phys. Rev. B **54**, 15762 (1996).
[57] H. Wendt and R. Richert, J. Phys. IV **10**, Pr7-67 (2000).
[58] E. W. Fischer, E. Donth, and W. Steffen, Phys. Rev. Lett. **68**, 2344 (1992).
[59] U. Tracht, M. Wilhelm, A. Heuer, H. Feng, K. Schmidt-Rohr, and H. W. Spiess, Phys. Rev. Lett. **81**, 2727 (1998).
[60] C. Donati and J. Jäckle, J. Phys.: Condens. Matter **8**, 2733 (1996).
[61] P. Scheidler, W. Kob, and K. Binder, Europhys. Lett. **52**, 277 (2000).
[62] C. Burger, Ph.D. thesis, Marburg University, Germany, 1994.
[63] R. Richert and M. Richert, Phys. Rev. E **58**, 779 (1998).
[64] D. Morineau, Y. Xia, and C. Alba-Simionesco, J. Chem. Phys. **117**, 8966 (2002).
[65] J. Schüller, Y. B. Mel'nichenko, R. Richert, and E. W. Fischer, Phys. Rev. Lett. **73**, 2224 (1994).
[66] W. Gorbatschow, M. Arndt, R. Stannarius, and F. Kremer, Europhys. Lett. **35**, 719 (1996).
[67] P. Pissis, A. Kyritsis, D. Daoukaki, G. Barut, R. Pelster, and G. Nimtz, J. Phys.: Condens. Matter **10**, 6205 (1998).
[68] M. Arndt, R. Stannarius, W. Gorbatschow, and F. Kremer, Phys. Rev. E **54**, 5377 (1996).
[69] T. Sasaki, A. Shimizu, T. H. Mourey, C. T. Courtney, and M. D. Ediger, J. Chem. Phys. **119**, 8730 (2003).
[70] C. A. Angell, R. K. Kadiyala, and D. R. MacFarlane, J. Phys. Chem. **88**, 4593 (1984).
[71] J. L. Green, J. Phys. Chem. **94**, 5647 (1990).
[72] L.-M. Wang and R. Richert, J. Chem. Phys. **120**, 11082 (2004).
[73] J. C. Deak, Y. Pang, T. D. Sechler, Z. Wang, and D. D. Dlott, Science **306**, 473 (2004).
[74] M. Yanagimachi, N. Tamai, and H. Masuhara, Chem. Phys. Lett. **200**, 469 (1992).
[75] A. Scodinu, R. A. Farrer, and J. T. Fourkas, J. Phys. Chem. B **106**, 12863 (2002).
[76] B. J. Loughnane, A. Scodinu, and J. T. Fourkas, J. Phys. Chem. B **103**, 6061 (1999).
[77] R. A. Farrer, B. J. Loughnane, and J. T. Fourkas, J. Phys. Chem. A **101**, 4005 (1997).
[78] S. Takahara, O. Yamamuro, and T. Matsuo, J. Phys. Chem. **99**, 9589 (1995).
[79] B. J. Loughnane, R. A. Farrer, A. Scodinu, T. Reilly, and J. T. Fourkas, J. Phys. Chem. B **104**, 5421 (2000).